Available online at www.sciencedirect.com
ScienceDirect
Journal of Power Sources 162 (2006) 1289–1296
JOURNAL OF POWER SOURCES
www.elsevier.com/locate/jpowsour

Kinetic behavior of $LiFeMgPO_4$ cathode material for Li-ion batteries

Jian Hong, Chunsheng Wang *, Uday Kasavajjula

Center for Manufacturing Research, Department of Chemical Engineering, Tennessee Technological University, Cookeville, TN 38505, United States

Received 21 July 2006; received in revised form 31 July 2006; accepted 1 August 2006
Available online 8 September 2006

Abstract

$LiFe_{0.9}Mg_{0.1}PO_4$ material was prepared by mechanical milling method, followed by heat treatment. The equilibrium potential-composition isotherm of $LiFe_{0.9}Mg_{0.1}PO_4$ and charge–discharge kinetics of $LiFe_{0.9}Mg_{0.1}PO_4$ were measured using galvanostatic intermittent titration technique (GITT), potential-step chronoamperometry (PSCA), and electrochemical impedance spectroscopy (EIS). The rate performance of the cathode is controlled by the charge-transfer kinetics, electronic conductivity, Li-ion diffusion capability, and phase transformation rate. Since $LiFe_{0.9}Mg_{0.1}PO_4$ has a fast charge-transfer reaction and high electronic and ionic diffusivity, the phase transformation between $LiFe_{0.9}Mg_{0.1}PO_4$ and $Li_{0.1}Fe_{0.9}Mg_{0.1}PO_4$ begins to play a more important role in the charge–discharge process, as is evident by an inductive loop induced by the phase transformation in the low frequency region of EIS. The phase purity and morphology of $LiFe_{0.9}Mg_{0.1}PO_4$ were also observed using X-ray diffraction (XRD) and scanning electron microscopy (SEM).

Keywords: Li-ion batteries; $LiFePO_4$; Kinetics; Electrochemical impedance spectroscopy

1. Introduction

Lithium iron phosphate ($LiFePO_4$) is one of the most promising cathode materials for Li-ion batteries because of its large theoretical capacity, low cost, and it's environmentally friendly nature. $LiFePO_4$ has olivine oxy-anion scaffolded-structures built from corner-sharing MO_6 octahedral and XO_4^{n-} tetrahedral anions [1]. Olivine is regarded as a stable structure for Li-insertion/extraction and should have good cycling stability [2]. However, the pristine compound has a disadvantage of poor rate performance due to its low electronic conductivity ($\sim 10^{-9}$ S cm^{-1}). Several methods have been reported to enhance the inherent electronic conductivity, including carbon coating [3], super-valence ion doping in Li-site [4], and nano-networking of electronic conductive metal-rich phosphide formed under reduction (5% H_2) atmosphere at high temperatures [5]. Using these methods, one can get uniformly doped materials with electronic conductivity as high as 4.8×10^{-2} S cm^{-1} [4,6]. However, it seems that the improved electronic conductivity did not improve $LiFePO_4$ performance as expected. From these results it seems that other than electronic conductivity, material properties such as ionic conductivity and phase transformation may have strong influence on rate capability. Yamada et al. [7] reported that the increasing the specific surface area by uniform dispersion of fine particles in the electrode has resulted in better electrochemical performance. This improvement was attributed to the short diffusion distance in the fine $LiFePO_4$ particles. Recently, it has been reported that the rate capability and cyclic stability of $LiFe_{0.9}M_{0.1}PO_4$ (M = Ni, Co, and Mg) can be greatly enhanced by bivalent cation doping at Fe-site [8]. Under a high discharge current of 10 C, $LiFe_{0.9}Mg_{0.1}PO_4$ showed similar capacity as $LiFe_{0.9}Co_{0.1}PO_4$ (90 mA h g^{-1}), but higher than that of $LiFe_{0.9}Ni_{0.1}PO_4$ (82 mA h g^{-1}) [8]. Fe-site doping probably weakens the Li–O interaction, resulting in high ionic mobility and diffusion coefficient [8]. Though the extremely flat charge–discharge profile is categorized as typical of two-phase reaction systems, which is the key feature of the $LiFePO_4$ cathode, only few researchers have discussed the importance of phase transformation in $LiFePO_4$ during charge–discharge process [7–10]. For the charge–discharge simulation of $LiFePO_4$, a core–shell reaction scheme has been applied, assuming a shrinking core with the movement of the $Li_\alpha FePO_4$ (heterosite phase)–$Li_{1-\beta}FePO_4$ (triphylite phase) interface [10–13], where the values of α and β are both approximately 0.03–0.04 [9]. So far, all the mathematical models used for determining the

* Corresponding author.
E-mail address: cswang@tntech.edu (C. Wang).

0378-7753/$ – see front matter © 2006 Elsevier B.V. All rights reserved.
doi:10.1016/j.jpowsour.2006.08.004

charge–discharge behavior of electrode materials are based on the assumption that the charge–discharge process is controlled by diffusion. However, recent results show that the phase transformation of electrodes (for example graphite anode) may control the charge–discharge process of the electrodes especially at the initial stage [14] because the stress and stain induced by phase transformation decreases the rate of phase transformation [15]. It is found that the electrodes with the low volume change during Li insertion/extraction have a high rate capability. For example, the $Li_4Ti_5O_{12}$ with almost zero volume change has excellent rate capability due to the fast phase transformation. Therefore, the phase transformation may play an important role in charge–discharge process of electrode.

Electrochemical impedance spectroscopy (EIS) is a very powerful technology to determine the rate of individual electrode kinetic steps, if their time constants are resolvable [16]. Normally, EIS will be measured over a certain frequency range at a potentiostatic signal amplitude of 5 mV. The use of small amplitude perturbations is to meet the linearity requirement for accurate EIS measurement in the real electrochemical systems. The 5 mV potentiostatic signal is normally smaller than the equilibrium potential hysteresis induced by the phase transformational strain (for example, the equilibrium potential hysteresis of graphite is around 10–30 mV in the state transformation regions [17,18]). Therefore, the phase transformation will not be detected by EIS. However, when the driving-force induced by the potential bias in the EIS measurement is larger than the critical force needed (energy barrier) for phase transformation, the phase transition will occur during EIS measurement, which may change the nature of impedance spectra. Therefore, the EIS with large potential bias also can be used to investigate the phase transformation kinetics.

Another useful method for investigating the kinetics of Li diffusion and phase transformation is potential-step chronoamperometry (PSCA), which was successfully used for understanding the charge–discharge behavior of graphite anodes [15,19].

In this paper, we made an effort to understand the effect of phase transformation on the reaction kinetics of $LiFe_{0.9}Mg_{0.1}PO_4$ in two-phase regions by two different experimental techniques i.e. potential-step chronoamperometry and EIS with different potentiostatic signal amplitudes. The reason to select $LiFe_{0.9}Mg_{0.1}PO_4$ material is because it shows both a high Li-ion diffusion ability and an electronic conductivity [8], and the phase transformation during the charge and discharge may be a controlling step for its rate capability.

2. Experimental

2.1. Synthesis and characterization of $LiFe_{0.9}Mg_{0.1}PO_4$

The $LiFePO_4$ powder sample was prepared by a process designed to reduce the impedance of materials for both electrons and ions. In this process, Li_2CO_3 (Aldrich, 99%), $FeC_2O_4{\cdot}2H_2O$ (Aldrich, 99%), $NH_4H_2PO_4$ (Aldrich, 99%), and $MgC_2O_4{\cdot}2H_2O$ (Alfa, 95%) were thoroughly mixed (ratio of Li:Fe:P:Mg = 1:0.9:1:0.1) using mechanical milling (Spex 8000M Mixer/Mill) and then followed by mechanical milling in the acetone solution for 24 h. After the precursors were dried in air, they were reacted in Argon gas (with 5% H_2) at 350 °C for 5 h and at 700 °C for 8 h in a Lindberg tube furnace equipped with mass flow controllers. The heat treatment under reduction atmosphere (Ar + 5% H_2) is to form an nano-networking of highly electronic conductive Fe_2P. After firing, the final powders were sieved. The crystalline phases of doped $LiFe_{0.9}Mg_{0.1}PO_4$ powders were identified by X-ray diffraction using a Rigaku AFC5 diffractometer with a Cu Kα radiation. The diffraction data was collected at 0.02 (degree sign) step width over a 2θ range from 10° to 90°. The particle size was observed by scanning electron microscopy (SEM) images using a FEI Quanta 200 equipped with energy dispersive spectroscopy (EDS).

The $LiFe_{0.9}Mg_{0.1}PO_4$ pellet used for the electronic conductivity measurement was prepared by die-pressing $LiFe_{0.9}Mg_{0.1}PO_4$ powders (without carbon and binders) with a pressure of 3 tonnes cm^{-2}, and then coating with Ag paste on both sides. The size of the pellet was around 1.3 cm diameter with 0.06 cm thickness. The electronic conductivity of $LiFe_{0.9}Mg_{0.1}PO_4$ was measured by both linear polarization using Solartron 1287 and EIS using Solartron 1287/1260.

2.2. Electrochemical performance of $LiFe_{0.9}Mg_{0.1}PO_4$

The electrode used for testing the electrochemical performance consisted of 88% $LiFe_{0.9}Mg_{0.1}PO_4$ powder, 6% carbon black, and 6% polyvinylidene fluoride (Kynar™, Elf-Atochem) in 1-methyl-2-pyrrolidinone solvent. The mixture prepared from above composition was coated onto Al mesh current collectors to form a disk electrode with 20 mg cm^{-2} density of active material (geometric surface area of 1.5 cm^2 containing 30 mg $LiFe_{0.9}Mg_{0.1}PO_4$). After drying in oven at 120 °C, the disk electrodes were pressed with a pressure of 1 tonnes cm^{-2} for 10 min. Electrochemical measurements were performed at room temperature in a three-compartment PTFE cell of conventional design, with lithium foil as counter and reference electrodes (Fig. 1). All the cells contained 1.0 M $LiPF_6$ in EC–DEC–DMC–EMC (1:1:1:3 by volume) (Ferro Corporation) as electrolyte and were assembled in an argon-filled glove box. Charge and discharge characteristics were performed between 2.5 and 4.2 V

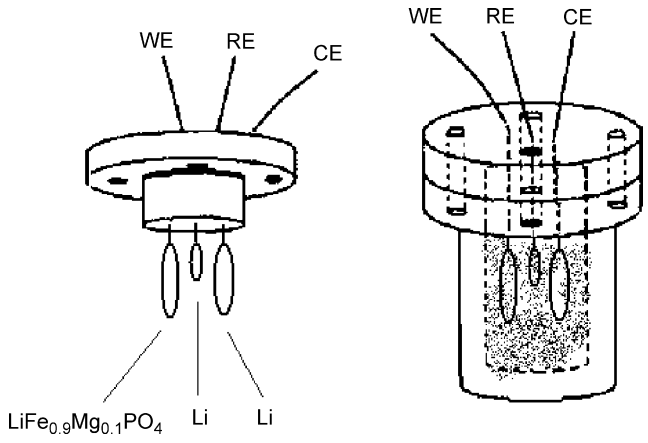

Fig. 1. PTFE cell configuration for the charge/discharge and the electrochemical impedance spectroscopy measurements of the $LiFe_{0.9}Mg_{0.1}PO_4$ electrodes.

using Arbin Corporation (College Station, TX) automatic battery cycler. The Li insertion/extraction equilibrium potential-composition isotherm of $LiFe_{0.9}Mg_{0.1}PO_4$ was measured by galvanostatic intermittent titration technique (GITT) [16]. The $LiFe_{0.9}Mg_{0.1}PO_4$ was charged and discharged by the use of series of intermittent current at 2 mA g^{-1} for 1.0 h, leaving the electrode at open circuit for 2.0 h between each intermittent current. The open-circuit potential after 2.0 h relaxation as a function of Li content was obtained.

The electrochemical reaction kinetics of $LiFe_{0.9}Mg_{0.1}PO_4$ were measured using Solartron FRA 1260 frequency response analyzer with a Solartron Model 1287 electrochemical interface within the frequency range of 10^6 Hz to 1.0 mHz and at potentiostatic signal amplitudes of 5, 10, 20 and 30 mV, respectively. The electrochemical reaction impedances were measured after Li was inserted or extracted to desired levels, followed by keeping at open circuit for 1.0 h for potential stabilization. The potential-step chronoamperometry was performed by stepping the potential from 3.6 to 3.1 V or from 3.1 to 3.48 V after the electrode was equilibrated for 2 h. During the potential jump, a phase transformation between $LiFe_{0.9}Mg_{0.1}PO_4$ and $Li_{0.1}Fe_{0.9}Mg_{0.1}PO_4$ takes place. The negative charge current induced by potential jump from 3.1 to 3.48 V was converted to positive value to compare with discharge current jump.

3. Results and discussion

3.1. Structural properties

The $LiFe_{0.9}Mg_{0.1}PO_4$ powders were analyzed by XRD to verify phase purity as shown in Fig. 2. The prepared $LiFe_{0.9}Mg_{0.1}PO_4$ is found to have well-crystallized orthorhombic structure. There is a good correspondence with the reference $LiFePO_4$ pattern, demonstrating that there are no detectable impurity phases. Partial substitution of Fe^{2+} ions by Mg^{2+} resulted in slight change in the cell size, without forming a new phase. The XRD pattern of prepared $LiFe_{0.9}Mg_{0.1}PO_4$ is in agreement with reported structure of $LiFe_{0.9}Mg_{0.1}PO_4$ [8]. It was reported that the substitution of 10% of Fe^{2+} ions by

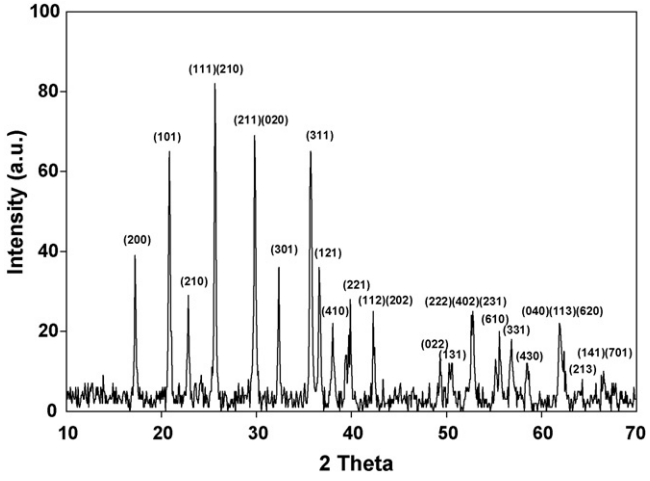

Fig. 2. The X-ray pattern of $LiFe_{0.9}Mg_{0.1}PO_4$.

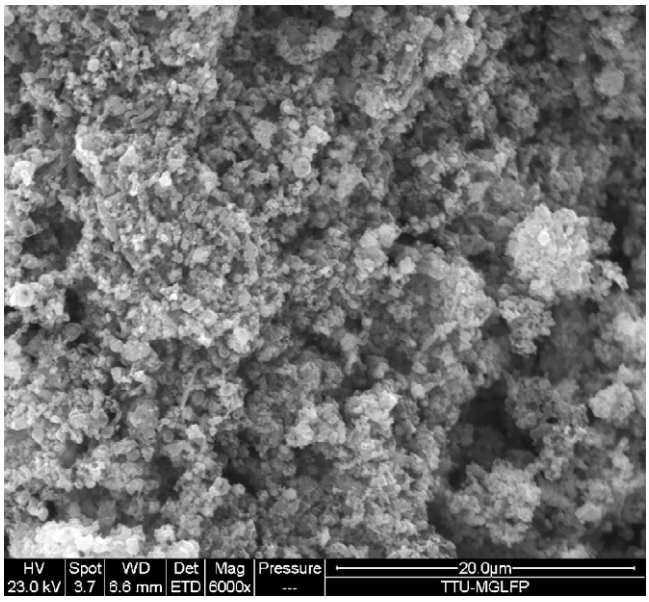

Fig. 3. The SEM image of $LiFe_{0.9}Mg_{0.1}PO_4$.

Mg^{2+} ions shrinks the *a*-, *b*-, and *c*-axis of olivine $LiFePO_4$ by 0.13%, 0.23%, 0.02%, respectively [8]. The morphologies of $LiFe_{0.9}Mg_{0.1}PO_4$ are shown in Fig. 3. The powders have an aggregate particle size of less than 1 μm. The individual particle size may be much less than 1 μm.

3.2. Li insertion/extraction equilibrium potential-composition isotherm of $LiFe_{0.9}Mg_{0.1}PO_4$

Fig. 4 shows the galvanostatic intermittent charge/discharge curves for $LiFe_{0.9}Mg_{0.1}PO_4$ measured at 25 °C with a successive charge/discharge at a current density of 2 mA g^{-1} for 2 h followed by 2.0 h of resting time (on open circuit). The reversible capacity of $LiFe_{0.9}Mg_{0.1}PO_4$ is about 148 mA h g^{-1}, which is close to theoretical value of 156 mA h g^{-1} of $LiFe_{0.9}Mg_{0.1}PO_4$ [20]. The equilibrium potential hysteresis of $LiFe_{0.9}Mg_{0.1}PO_4$

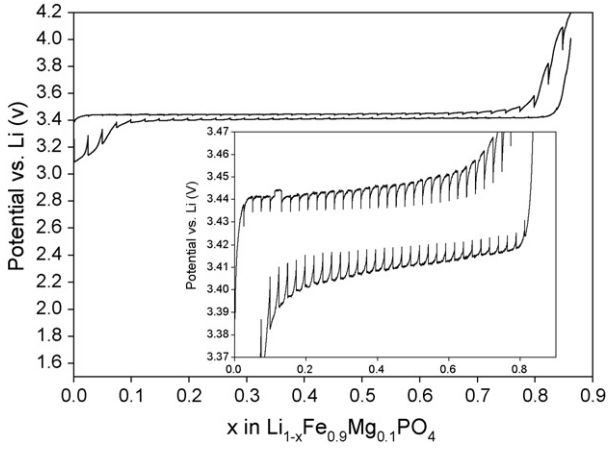

Fig. 4. Galvanostatic intermittent charge/discharge curves for $LiFe_{0.9}Mg_{0.1}PO_4$ measured at 25 °C with a successive charge–discharge current at 2 mA g^{-1} for 2 h followed by 2.0 h at open circuit. Inserted figure is an enlarged PCI curve in the two-phase region.

between Li insertion and extraction is about 18 mV. Interestingly, the overpotential in the two-phase region increased (from 8 to 12 mV) with the increase of Li insertion or extraction, which is attributed to the increased diffusion length according to shrinking core model [16].

3.3. Rate capability

$LiFe_{0.9}Mg_{0.1}PO_4$ electrode has shown 68% of the capacity even at 10 C discharge rate, which shows its excellent rate capability (Fig. 5). This is due to the fast electrochemical reaction kinetics of $LiFe_{0.9}Mg_{0.1}PO_4$. The IR drops during high-rate discharge in the two-phase (the flat plateau) region depends strongly on the discharge current. This polarization may be induced by the resistance related to ohm drop, charge-transfer, Li^+ diffusion, and phase transformation of the electrode.

3.4. Potential-step chronoamperometry (PSCA) measurement

To determine Li^+ ion diffusivity in $LiFe_{0.9}Mg_{0.1}PO_4$, current–transient response of $LiFe_{0.9}Mg_{0.1}PO_4$ was tested using potential-step chronoamperometry (PSCA) measurement. Fig. 5 shows the current–transient curves for $LiFe_{0.9}Mg_{0.1}PO_4$ obtained by potential-step from open-circuit potential (OCP) 3.6 to 3.1 V, and from OCP 3.1 to 3.48 V, in which the phase transformation between $LiFe_{0.9}Mg_{0.1}PO_4$ and $Li_{0.1}Fe_{0.9}Mg_{0.1}PO_4$ took place. The current decayed rapidly in both cases, although the initial current and decay rate are different for the two potential jumps (Fig. 6a). The slightly higher current for discharge (from 3.6 to 3.1 V) than that for charge (from 3.1 to 3.48 V) is probably due to large potential jump (0.5 V) in the discharge. A current hump was found for each potential jump after an initial rapid decay of the current. The presence of these current humps is the characteristic of nucleation in the phase transformation [19,21], which suggests that electrochemical nucleation and growth are involved in the electrode reaction at least during the initial stages [19]. To determine the controlling step, the linear scale in Fig. 6a was converted into logarithm scale and replotted in Fig. 6b. If diffusion controls the electrode reaction, a linear relationship between the logarithm of current and the logarithm of time with an absolute of 0.5 (i.e. Cottrell behavior) will be observed before an exponential decay of current with time [22]. However, the slope in Fig. 6b is lower in absolute value than 0.5 in the early stage, which suggests that the Li^+ diffusion in the $LiFe_{0.9}Mg_{0.1}PO_4$ is not the controlling step. To further ascertain that diffusion is not a controlling step, the position of the phase boundary between $Li_{0.1}Fe_{0.9}Mg_{0.1}PO_4$ and $LiFe_{0.9}Mg_{0.1}PO_4$ as a function of charge time was calculated based on shrinking core model (Fig. 7) proposed by Srinivasan and Newman [11] for $LiFePO_4$ electrode. Using the shrinking core model [11,19], position of the phase boundary can be calculated from reacted fraction (Q_t/Q_∞), and

$$\xi = r_0 \left[1 - \left(1 - \frac{Q_t}{Q_\infty} \right)^{1/3} \right] \tag{1}$$

The reacted fraction Q_t/Q_∞ in Eq. (1) can be determined by the ratio of charge passed for a specific time (t) to the total charge, which is as follows:

$$\frac{Q_t}{Q_\infty} = \alpha = \frac{\int_0^t I(t)\,\mathrm{d}t}{\int_0^\infty I(t)\,\mathrm{d}t} \tag{2}$$

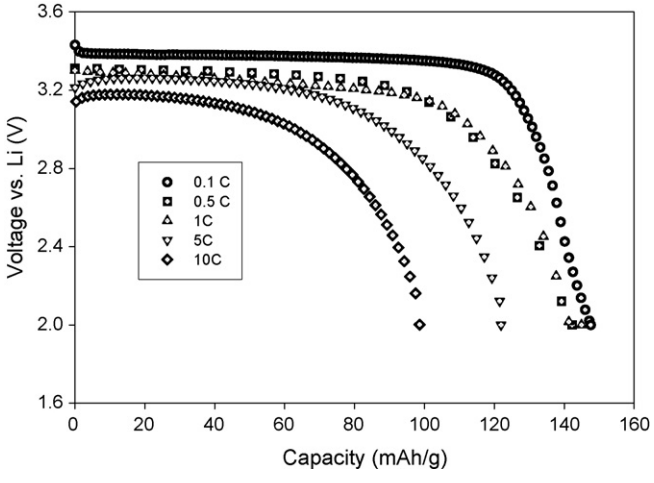

Fig. 5. The discharge curves of $LiFe_{0.9}Mg_{0.1}PO_4$ under different discharge current (C rate).

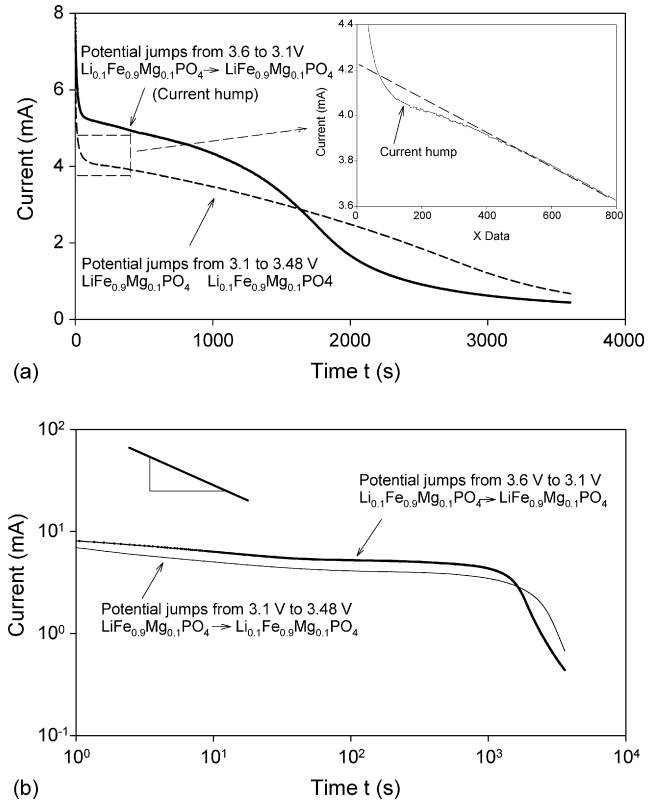

Fig. 6. The absolute value of anodic and cathodic currents of $LiFe_{0.9}Mg_{0.1}PO_4$ (a) in a linear scale and (b) in a logarithm scale obtained by potential-step experiment. The negative charge current induced by potential jump from 3.1 to 3.48 V was converted to positive value to compare with discharge current jump.

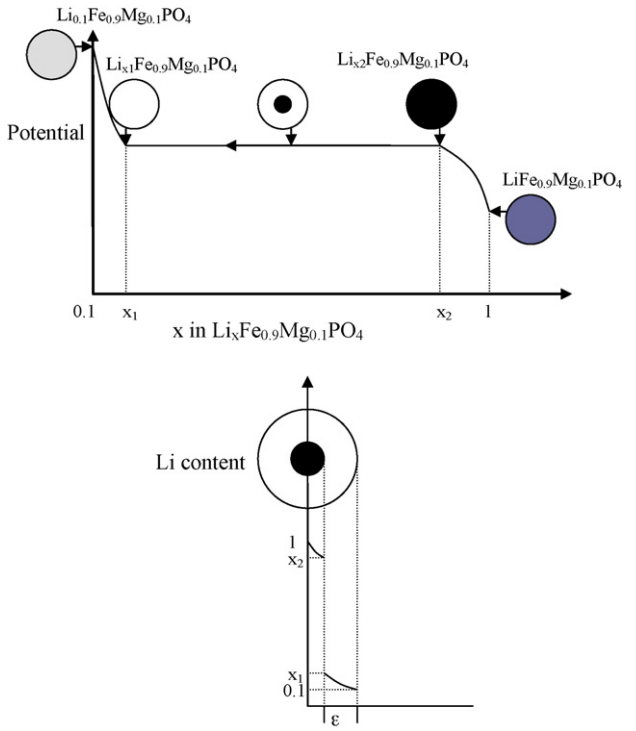

Fig. 7. Illustration of the shrinking-core model with the juxtaposition of the two-phases during the Li extraction from $LiFe_{0.9}Mg_{0.1}PO_4$ and the movement of the phase boundary.

where r_0 is the radius of the particle and ξ is the position of phase boundary.

From the $I(t)$ versus time plot obtained from PSCA measurements during charge process, reacted fraction values were computed using Eq. (2). Fig. 8 shows the variation of experimentally determined α values with time t. From the plot, the total reaction time was found to be 57 min. From the variation of experimentally determined values of α with time (Fig. 8),

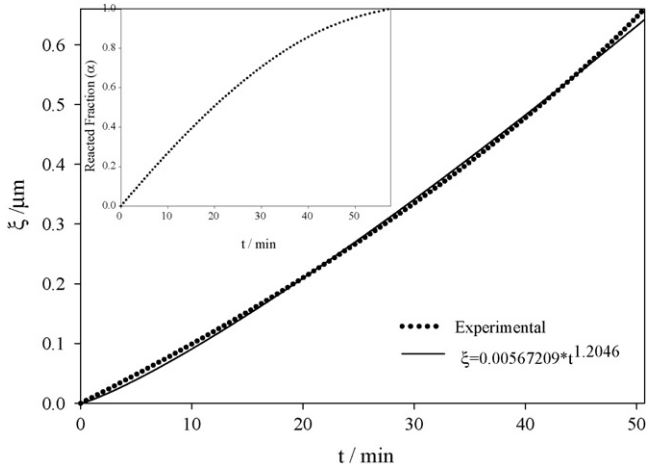

Fig. 8. Relationship between the position of phase boundary ξ and time for $LiFePO_4$ electrode during charge process. (Inset: time dependence of reacted fraction $\alpha(t)$ of fully discharged $LiFe_{0.9}Mg_{0.1}PO_4$ electrode for the charge process.)

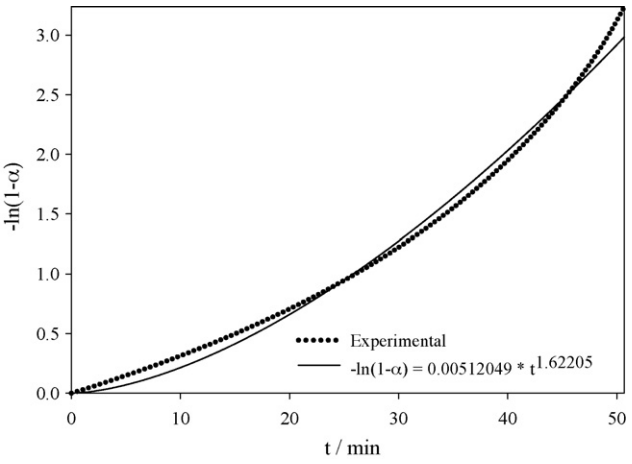

Fig. 9. $-\ln(1-\alpha)$ plotted against time for charge process of $LiFe_{0.9}Mg_{0.1}PO_4$ electrode.

the position of phase boundary for different time values was obtained using Eq. (1), which is also shown in Fig. 8. In Fig. 8, ξ versus t plot is found to be a straight line with a slope of 0.0154. If the reaction process is controlled by diffusion, ξ versus $t^{1/2}$ plot should be a straight line according to the Funabiki et al. [19] and Jost [23] analysis for a diffusion-limited phase transformation with a moving phase boundary. However, Fig. 8 shows a linear relationship with $t^{1.2}$ not $t^{1/2}$, which further confirms that the reaction process is not controlled by diffusion. If phase transformation (nucleation and growth) is the limiting step during the charge and discharge, fraction transformation or reacted fraction should follow the Johnson–Mehl–Avrami equation [24]:

$$\alpha = 1 - \exp(-kt^m) \tag{3}$$

The k ($k^{1/m}$ unit: s^{-1}) value in Eq. (3) depends on number of factors such as geometry of the growing nuclei, initial number of nuclei per unit volume, growth velocity of the nuclei, and dimensionality of growth [25]. Similarly the factor m depends on nucleation rate per unit volume and dimensionality of growth [25]. For convenience Eq. (3) can be written as

$$[-\ln(1-\alpha)]^{1/m} = k^{1/m}t \tag{4}$$

The experimental and fitted values of $-\ln(1-\alpha)$ and time were also shown in Fig. 9, which resulted in values of 3.9×10^{-3}, 1.6 for k and m, respectively (fitting was achieved with a R^2 value of 0.99233, which shows the accuracy of the fit). The m value obtained from the fit being greater than 1 also shows that the reaction rate is controlled by nucleation and growth mechanism, i.e. phase transformation [25].

3.5. Electrochemical impedance spectroscopy (EIS) measurements

EIS with different potentiostatic signal amplitudes was used to determine individual impedances of the reaction process, including that of the electrolyte, the passivation layer, charge-transfer, Li^+ diffusion and phase transformation because EIS can give the impedance of each step if the individual time constants are separable. Fig. 10 shows the impedances of $LiFe_{0.9}Mg_{0.1}PO_4$

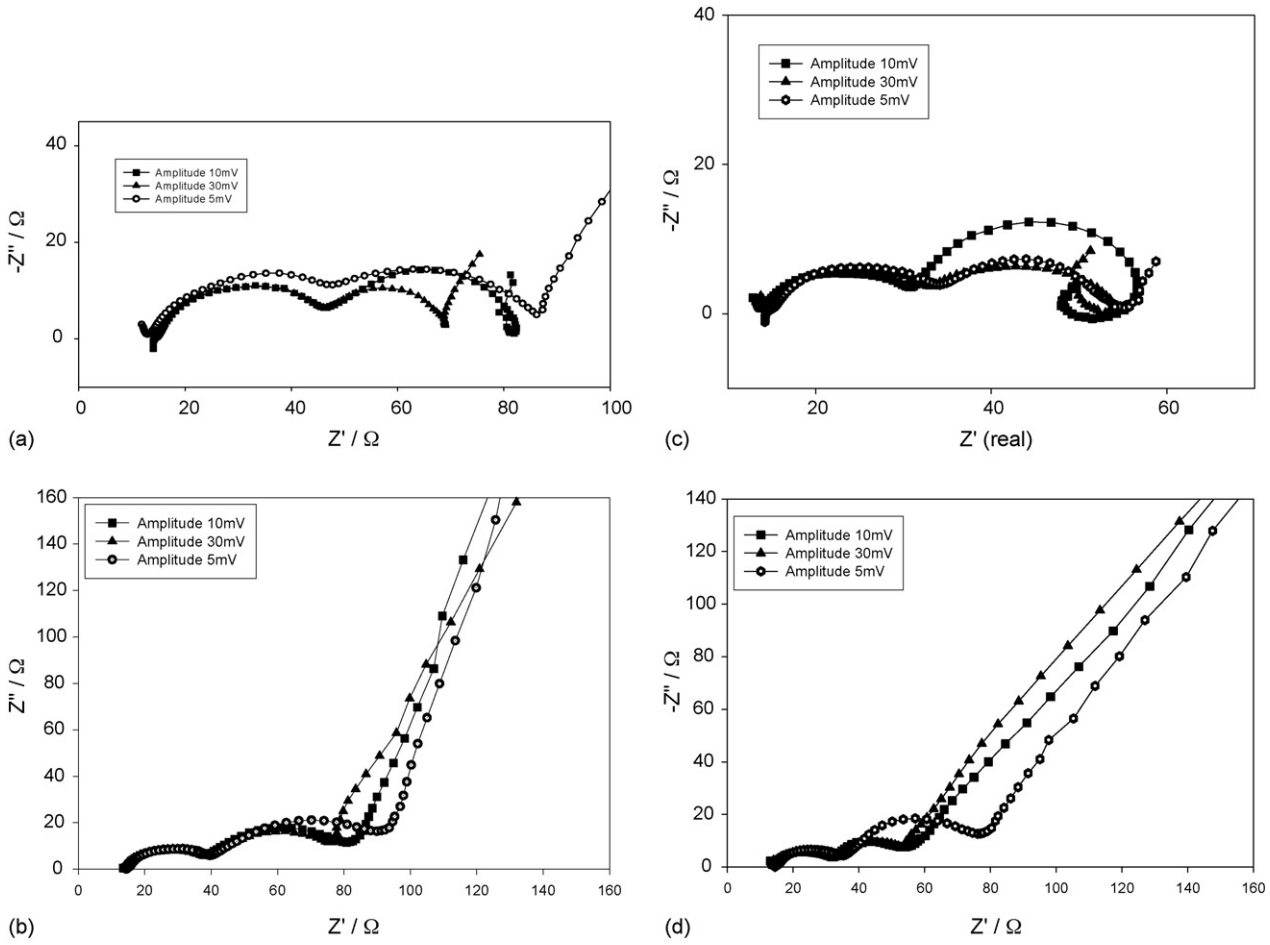

Fig. 10. The impedance of $LiFe_{0.9}Mg_{0.1}PO_4$ at (a) 50% state of charge ($V = 3.445$ V; two-phase region), (b) fully charge state ($V = 3.75$ V; single-phase region), (c) 50% state of discharge (3.41 V, two-phase region) and fully discharge state ($V = 3.2$ V; single-phase region).

obtained at 50% state of charge (3.45 V, two-phase region, Fig. 10a), fully charge (3.75 V, single-phase region, Fig. 10b), 50% state of discharge (3.41 V, two-phase region, Fig. 10c), and fully discharge (3.20 V, single-phase region, Fig. 10d), respectively. Before EIS measurement, the $LiFe_{0.9}Mg_{0.1}PO_4$ was charged–discharged for seven cycles for activation. Impedance in the single-phase regions, i.e. at the fully charge (Fig. 10b) and the fully discharge (Fig. 10d) stage, showed two semicircles at high frequency and a sloping line at the low frequency, which is common for cathode materials (such as $LiCoO_2$, and $LiFePO_4$). The first high frequency semicircle may be attributed to the solid electrolyte interphase (SEI) film formed during the first several charge–discharge cycles, and the second middle-frequency semicircle is probably due to charge-transfer reaction. The sloping line at the low frequency region is attributed to Li^+ diffusion in $LiFe_{0.9}Mg_{0.1}PO_4$. Moreover, the small magnitude of charge-transfer resistance (second semicircle), which is comparable with the resistance of SEI film (the first semicircle), suggests that charge-transfer reaction is very fast. The fast charge-transfer reaction is probably due to the high reaction area induced by the small particle size (Fig. 2). The small particle size also enhances the Li^+ diffusion capability due to the short diffusion path in $LiFe_{0.9}Mg_{0.1}PO_4$ particles. Increasing the potentiostatic signal amplitude from 5 to 30 mV did not influence the SEI film impedance, but slightly changes the charge-transfer resistance. The impedance in the two-phase regions (50% of state of charge, Fig. 5a and 50% of state of discharge, Fig. 5c) measured using 5 mV of potentiostatic signal amplitude are similar to the impedance in the single-phase region. However, with the increase of the signal amplitude to 10 and 30 mV, an inductive loop appeared in the low frequency region, which can be attributed to the phase transformation. This inductive loop is an intrinsic property of $LiFe_{0.9}Mg_{0.1}PO_4$, not an experimental artifact due to three-electrode configuration because the inductive loop exist only at large potentiostatic signal amplitude. Also, the PTFE cell configuration (Fig. 1) used to measure $LiFe_{0.9}Mg_{0.1}PO_4$ cathode is a typical and standard three-electrode cell. In addition, the EIS of other four $LiFe_{0.9}Mg_{0.1}PO_4$ cathodes were also measured in three-electrode PTFE cells and pouch cells using different instruments. Irrespective of the impedance equipment (Solartron and EG&G 2273) used, same results were obtained for all the samples. An inductive loop at a low frequency region is generally associated with consecutive heterogeneous reactions involving adsorption intermediates, such as pitting corrosion of metal, and methanol (or H_2/CO) oxidation [26] and surface capacities [27]. However, the adsorption intermediates cannot explain the inductive loop in this work because there is no adsorption intermediate during

Li insertion/extraction and the inductive loop only occurred in the phase transition region with a high potential bias. Therefore, the inductive loop occurred in the phase transformation region was confirmed to be an intrinsic property of $LiFe_{0.9}Mg_{0.1}PO_4$ cathode, and is related to the phase transformation.

During the phase transformation between $LiFe_{0.9}Mg_{0.1}PO_4$ and $Li_{0.1}Fe_{0.9}Mg_{0.1}PO_4$ there is a 6.5% volume change [9,28], and this leads to elastic–plastic deformation inside the materials. The irreversible processes of plastic deformation and dislocation generated during the phase transformation induce potential hysteresis (Fig. 4) [29]. Therefore, the phase transformation will occur only when the applied energy is higher than opposing elastic–plastic accommodation energy determined by the volume change in the phase transformation [29]. The driving force produced by 5 mV of potentiostatic signal amplitude in EIS measurement is probably smaller than that required force for the phase transformation, so no phase transformation has occurred and the interface between $LiFe_{0.9}Mg_{0.1}PO_4$ and $Fe_{0.9}Mg_{0.1}PO_4$ is stable during EIS measurement. This hypothesis is also supported by the fact that the potentiostatic signal amplitude (±5 mV) in EIS measurement is less than the equilibrium potential hysteresis in two-phase region (over 15 mV in Fig. 4). In this case, the impedance plot in two-phase region will be similar to that in the single-phase. However, when the potentiostatic signal amplitude increases to ±10 and ±30 mV, the induced driving force (energy) will be higher than the required force (energy) for phase transformation, the interface between two-phases will move accordingly during EIS measurement, which results in a inductive loop in the low frequency region (Fig. 10a and c). Another possibility is that the inductive loop may be induced by the non-linear behavior at the high potentiostatic signal amplitude. If so, the inductive loop will also appear in the single-phase region when potentiostatic signal amplitude is over 10 mV. However, no inductive loop occurred in the impedance plot measured at the single-phase region whatever the potentiostatic signal amplitudes were, 5, 10, or 30 mV. The slight decrease in the charge-transfer impedance at the high potentiostatic signal magnitude is probably due to non-linear behavior at the high overpotential because the interfacial response tends to show strong non-linear behavior when applied overpotentials are large [30].

The impedance of phase transformation limited by nucleation and growth was investigated by Millet and Dantzer [31]. The nucleation and growth rate of phase transformation can be expressed by Johnson–Mehl–Avrami equation (Eq. (3)). The calculated impedance of nucleation and growth shows a high frequency inductive loop along with a low-frequency capacitive behavior [31]. From our experimental results and results reported by Millet and Dantzer [31], the inductive loops in Fig. 10 can be really attributed to the phase transformation.

Recently, the origin and physical model of the inductive loop in the diffusion impedance for two-phase electrode has been proposed and discussed by Bisquert et al. [32]. Generally a local relaxation process exists for diffusion of ions in the active materials [32]. The diffusion of Li-ion in a core–shell (two-phases) particle will occur through a shell (outside layer) phase and it will be affected both by relaxation in the shell phase and by phase

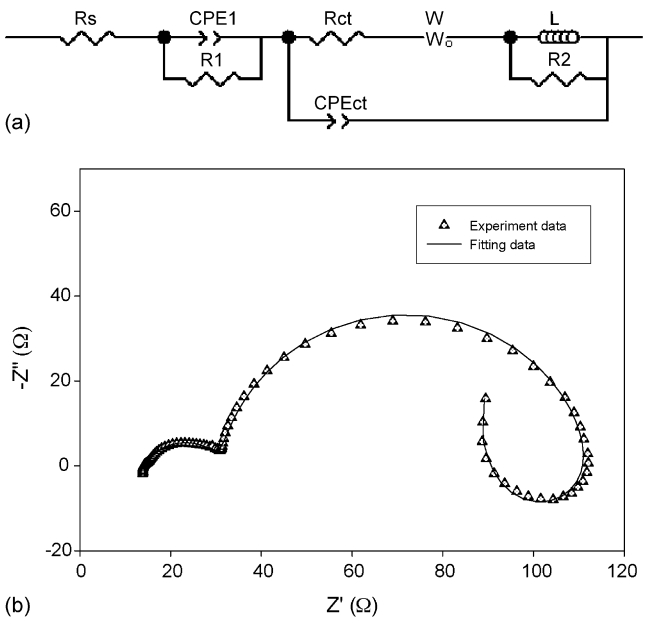

Fig. 11. The equivalent circuit (a) used to fit an experimental impedance curve (b) measured after discharging the $LiFe_{0.9}Mg_{0.1}PO_4$ electrode to 3.41 V vs. Li/Li^+. The fitted data are also shown in the figure for comparison.

transformation relaxation process (or trapping and detrapping from core phase). The coupling of two relaxations will cause an inductive feature in the high frequency region of diffusion impedance according to the theoretical calculation [32]. The intensity of inductive component is controlled by the ratio of the two relaxation times [32].

An equivalent circuit shown in Fig. 11 was used to analyze the measured impedance data. The impedance model involves three regions connected in series. The resistance R_S is used to simulate the contact resistance, electronic resistance in the electrode, and ionic conductive resistance in the electrolytes. The (CPE_1)–resistance (R_1) parallel elements are used to simulate the impedance of bulk electrode, and the CPE_{ct} paralleling with a resistance R_{ct} is for the impedance of charge-transfer reaction. W represents diffusion impedance. The phase transformation is simulated by an inductance L paralleled with a resistance (R_2). The CPE is a capacitive element usually related to the electrode roughness, inhomogeneous reaction rates n at surface, (e.g. polycrystalline metal surface or carbon electrodes with a distribution of active sites), and varying thickness or composition of a coating. Fig. 11 shows a typical impedance plot of the $Li_{1-x}Fe_{0.9}Mg_{0.1}PO_4$ measured at 50% state of discharge with the ac amplitude of 10 mV. The fit of the experiment was done with Z-plot and parameters values are presented in Table 1. We can find that the simulated curve fits the experimental data very well.

It should be mentioned that the inductive loop impedance occurs at the two-phase region only after it satisfies the following three criteria:

(1) The kinetics of electrode reaction is controlled by phase transformation or mixing controlled by phase transformation and diffusion. We tested the impedance of

Table 1
Values of the equivalent circuit components used for fitting the experimental curve

Components	Description	Fitted values
R_S	Solution resistance	14.5 Ω
R_1	The boundary resistance between two particles	17.07 Ω
CPE_1	Constant phase element of particle boundaries	1.36×10^{-4} F
R_{ct}	Resistance of the charge-transfer reaction	55.75 Ω
CPE_{ct}	Double layer capacitance	0.0025 F
L	Inductance	342 H
R_2	The resistance of the phase transformation	25.58 Ω

the $LiFe_{0.9}Mg_{0.1}PO_4$ with an electronic conductivity of 10^{-9} S cm^{-1}. There was no inductive loop impedance in the two-phase region even the potentiostatic signal amplitude is over 30 mV. Only the Warburg impedance was (a slop line) observed in the low frequency region.

(2) The applied driving force (potentiostatic signal amplitude) in the EIS measurement is high enough to overcome the resistance of the phase transformation.

(3) The electrode must be fully activated and stabilized by charging/discharging the electrode for several cycles. The impedance of $LiFe_{0.9}Mg_{0.1}PO_4$ cathode prepared in our lab was also measured during the first charging to the different Li levels. The inductive loop did not show up in all Li levels. After three charge–discharge cycles, the inductive loop impedance has appeared in two-phase region if the applied potentiostatic signal amplitude is over 10 mV. We tested the impedances of this $LiFe_{0.9}Mg_{0.1}PO_4$ sample at different Li levels in the 3rd, 7th and 30th charge–discharge cycles, the inductive loops appeared in the two-phase regions and disappeared in the single regions.

4. Conclusion

The structure and electrochemical performance of $LiFe_{0.9}Mg_{0.1}PO_4$ electrode have been investigated using XRD, SEM, GITT, PSCA and EIS. The prepared $LiFe_{0.9}Mg_{0.1}PO_4$ showed an equilibrium potential plateau in two-phase region with a potential hysteresis of 18 mV between Li insertion and extraction, and had a high rate capability. Due to the fast charge-transfer reaction and high electronic and ionic diffusivity, the phase transformation between $LiFe_{0.9}Mg_{0.1}PO_4$ and $Fe_{0.9}Mg_{0.1}PO_4$ begins to play an important role in the charge–discharge process. This was confirmed from the slope being less than 0.5 in PSCA measurement and the presence of inductive loop in the low frequency region of EIS. The phase transformation induced inductive loop appears in EIS only if (1) electronic, ionic diffusivity and charge-transfer reaction are fast, (2) the electrode is fully activated and (3) the applied driving force (potentiostatic signal amplitude) is large enough to move the phase boundary.

References

[1] H. Huang, S.C. Yin, L.F. Nazar, Electrochem. Solid State Lett. 4 (2001) A170.
[2] M. Takahashi, H. Ohtsuka, K. Akuto, Y. Sakurail, J. Electrochem. Soc. 152 (2005) A899.
[3] M.M. Doeff, Y. Hu, F. Mclarnon, R. Kostecki, Electrochem. Solid State Lett. 6 (2003) A207.
[4] S.Y. Chung, J. Bloking, Y. Ching, Nat. Mater. 1 (2002) 123.
[5] P.S. Herle, B. Ellis, N. Coombs, L.F. Nazar, Nat. Mater. 3 (2004) 147.
[6] S.Y. Chung, Y.M. Chiang, Electrochem. Solid State Lett. 6 (2003) A278.
[7] A. Yamada, S.C. Chung, K. Hinokuma, J. Electrochem. Soc. 148 (2001) A224.
[8] D. Wang, H. Li, S. Shi, X. Huang, L. Chen, Electrochim. Acta 50 (2005) 2955.
[9] A. Yamada, H. Koizumi, Z. Sonoyama, R. Kanno, Eelectrochem. Solid State Lett. 8 (2005) A409.
[10] A. Yamada, S.C. Chung, K. Hinokum, J. Electrochem. Soc. 148 (2001) A224.
[11] V. Srinivasan, J. Newman, J. Electrochem. Soc. 151 (2004) A1517.
[12] M. Yonemura, A. Yamada, Y. Takei, N. Sonoyyama, R. Kanno, J. Electrochem. Soc. 151 (2004) A1352.
[13] V. Srinivasan, J. Newman, Electrochem. Solid State Lett. 9 (2006) A110.
[14] A. Funabiki, M. Inaba, T. Abe, Z. Ogumi, J. Electrochem. Soc. 146 (1999) 2443.
[15] S.-I. Pyun, Y.-G. Ryu, J. Power Sources 70 (1998) 34.
[16] C. Wang, I. kakwan, A.J. Appleby, F.E. Little, J. Electroanal. Chem. 489 (2000) 55.
[17] J.R. Dahn, Phys. Rev. B 44 (1991) 9170.
[18] T. Ohzuku, Y. Iwakashi, K. Sawai, J. Electrochem. Soc. 140 (1993) 2490.
[19] A. Funabiki, M. Inaba, T. Abe, Z. Ogumi, J. Electrochem. Soc. 146 (1999) 2443.
[20] J. Barker, M.Y. Saidi, L. Swoyer, Electrochem. Solid State Lett. 6 (2003) A53.
[21] G. Gunawardena, G. Hills, I. Montenegro, B. Scharifker, J. Electroanal. Chem. 138 (1982) 225.
[22] J.W. Lee, S. Pyun II, Electrochim. Acta 50 (2005) 1777.
[23] W. Jost, Diffusion in Solid, Liquids, Gasses, Academic, New York, 1960 (Chapter I).
[24] D.A. Porter, K.E. Easterling, Phase Transformations in Metals and Alloys, 2nd ed., Stanley Thornes, UK, 1992 (Chapter 5).
[25] F. Feng, J. Han, M. Geng, D.O. Northwood, Sol. Energy Mater. Sol. Cells 62 (2000) 51.
[26] I.-M. Hsing, X. Wang, Y.J. Leng, J. Electrochem. Soc. 149 (2002) A615.
[27] G.F. Ortiz, R. Alcantara, P. Lavela, J.L. Tirado, Proceedings of the 208th ECS meeting on Modification of the Electrochemical Behavior of Carbon Nanofibers for Lithium-ion Batteries by Impregnation and Thermal and Hydrothermal Treatments, Los Angeles, 2005, p. 119.
[28] F. Zhou, M. Cococcioni, C.A. Marianetti, D. Morgan, G. Ceder, Phys. Rev. B 70 (2004) 235121.
[29] E. Rabkin, V.M. Skripnyuk, Scripta Mater. 49 (2003) 477.
[30] J.R. Macdonald, Impedance Spectroscopy, John Wiley and Sons, 1987, P2.
[31] P. Millet, P. Dantzer, Electrochem. Commun. 1 (1999) 163.
[32] J. Bisquert, H. Randriamahazaka, G. Garcia-Belmonte, Electrochim. Acta 51 (2005) 627.